ELEVENTH EUROPEAN ROTORCRAFT FORUM

Paper No. 24

APPLICATION OF A LIFTING SURFACE THEORY FOR A HELICOPTER IN FORWARD FLIGHT

Harry L. Runyan
The College of William and Mary
Williamsburg, Virginia

Hsiang Tai
NASA Langley Research Center
Hampton, Virginia

September 10-13, 1985
London, England

THE CITY UNIVERSITY, LONDON, EC1V OHB, ENGLAND.

APPLICATION OF A LIFTING SURFACE THEORY FOR A HELICOPTER IN FORWARD FLIGHT

Harry L. Runyan
The College of William and Mary
Williamsburg, Virginia

Hsiang Tai
NASA Langley Research Center
Hampton, Virginia

ABSTRACT

A lifting surface theory has been developed for a helicopter rotor in forward flight for compressible and incompressible flow. The method utilizes the concept of the linearized acceleration potential and makes use of the doublet lattice procedure. Calculations demonstrating the application of the method are given in terms of the lift distribution on a single rotor, a two-bladed rotor, and a rotor with swept-forward and swept-back tips. In addition, the lift on a rotor which is vibrating in a pitching mode at 4/rev is given. Compressibility effects and interference effects for a two-bladed rotor are discussed.

INTRODUCTION

The aerodynamic environment in which a helicopter rotor operates is very severe. In forward flight, the aerodynamic loads are time dependent and the wake from preceeding blades induces large interference effects. In high speed flight, the retreating blade usually stalls. The resulting dynamic loads plus others are acting on a long slender blade inducing high dynamic stresses and vibration modes.

The standard procedure for predicting the airloads on a rotor blade is to utilize experimentally derived, two-dimensional airforces which were obtained through a large range of angles of attack up to and through the stalled region. These data are usually put in tabular form and used in an iteration procedure to determine stability and performance. This process neglects the effect of the wake as well as the three-dimensional effects. Approximations are usually made to try to correct for the wake and the three-dimensional flow effects.

There are several analytical approaches that can be used to predict these unsteady airloads. Two traditional methods involve the use of the velocity potential or the acceleration potential. Runyan (1973) utilized the acceleration potential approach to obtain a solution for the oscillating propeller in compressible flow. Suciu et al (1976) have derived an incompressible lifting surface theory and applied it to a windmill. The procedure is based on the velocity potential method and subdivides the integration areas into panels within which a constant pressure distribution is assumed. Dat, (1973) has derived a general expression for an acceleration doublet for any motion. The theory developed by Dat was applied to a helicopter in forward flight by Costes (1972). Costes' approach is similar to the method given in this paper with the exception of a numerical

differentiation procedure which was adopted to obtain the downwash velocity from the velocity potential. In the present approach, the downwash velocity expression is obtained analytically. Pierce and Vaidyanathan (1983) have treated the helicopter rotor in forward flight using the method of matched asymptotic expansion for the incompressible case, which was based on the work of Van Holten (1975).

The method presented in this report sets forth a formulation of fundamental, three dimensional, compressible, unsteady aerodynamic theory for propellers and helicopter rotors in forward flight. An inertial coordinate system is adopted and the integrations involved in solving the integral equation are formulated for arbitrary space-time variations. In this formulation, singular terms arise in the integrations, which are handled by the finite part technique.

The paper is divided into three basic sections. The first section contains a brief derivation of the fundamental equations, which is followed by a section describing a method for solving the integral equation. Finally, the method is applied to specific examples and the computational results are given.

SYMBOLS

A'	rotor blade area
A_{nm}	aerodynamic influence coefficients
A_n, B_n	Fourier coefficients
c	speed of sound
C	chord of rotor
C_T	thrust coefficient (thrust/$\pi\rho\Omega^2 R_t^4$) where thrust is normal to tip path plane, and is positive in positive z-direction
$\vec{D}$	radius vector from doublet to downwash point
D	absolute value of $\vec{D}$
$\hat{D} = \vec{D}/D$	unit vector of $\vec{D}$
K	kernel function
$\vec{n}$	unit vector at downwash point, normal to velocity vector surface
$\vec{n}_o$	unit vector at doublet point, normal to velocity surface
p	pressure
$\vec{X}_o$	position vector of doublet from inertial frame origin
$\vec{X}$	position vector of downwash point from inertial frame origin
q	source or doublet strength
R_t	rotor tip radius
R_s	rotor root radius
r	distance to downwash point along the span
r_o	distance to doublet along the span
$\hat{r}_o$	distance to doublet along span at singular point time
t	field time
U	velocity of rotor system, parallel to x-axis, positive in negative x-direction

$\vec{V}$	velocity at downwash points
V_n	resultant velocity normal to blade
$\vec{V}_o$	velocity of doublet
W	velocity of rotor system, parallel to z axis
w_n	downwash velocity, normal to velocity plane, positive down
x,y,z	Cartesian coordinates of downwash point
x_o,y_o,z_o	Cartesian coordinates of doublet position
α	twist angle at downwash point
α_o	twist angle at doublet position
α_r	angle of axis of rotation relative to z-axis
$\vec{\beta}$	$\vec{V}_o/c$
$\dot{\vec{\beta}}$	$\dot{\vec{V}}_o/c = \frac{1}{c}\frac{\partial \vec{V}_o}{\partial \tau}$
θ	angular position of blade at time t ($\theta = \Omega t$)
θ_o	angular position of blade at time τ ($\theta_o = \Omega\tau$)
μ	advance ratio ($U/\Omega R_t$)
ρ	air density
τ, τ_o	source time
$\hat{\tau}$	source time at which integrand in Eq. 17 becomes singular
φ	velocity potential
Ψ	acceleration potential
ψ	azimuth angle measured from downwind position
Ω	rotation speed of rotor

BASIC FORMULATION

The formulation of the aerodynamic equations is based on the linearized acceleration potential approach. The fluid is considered perfect, with no separation and the formulation is based upon the assumption of small perturbations. One reason for adopting the acceleration potential approach is that the pressure discontinuity occurs only on the surface of the blade and thus the boundary conditions need only be applied on the blade surface and not throughout the wake. The blade is treated as a very thin surface of discontinuity across which a pressure jump occurs. The effect of compressibility is taken into account by utilizing the complete linearized potential for a lifting doublet, along with the effects of retarded time.

As shown in figure 1 an inertial coordinate system has been used. The helicopter rotor is moving in the negative x-direction with velocity U, in the positive z-direction with velocity W and is rotating counter clockwise with a constant angular velocity Ω. A point of interest on the rotor blade is designated by the vector $\vec{X}_o(\tau)$ from the origin of the ground based coordinate system.

Let Ψ be the acceleration potential of a source (or doublet),the perturbation pressure is then given by

$$p = -\rho\Psi \tag{1}$$

This expression represents the pressure p at point $\vec{X}$ due to a single source (or doublet) located at $\vec{X}_o$. The potential Ψ

contains a constant "q" which represents the strength of the source and thus the magnitude of the pressure. In this form, there is no boundary condition available to determine the value of the arbitrary constant "q" and the resulting pressure. Recourse can be made to the velocity potential, since the spatial derivative of a velocity potential represents a velocity. The relationship between the pressure and velocity potential for an inertial coordinate system is

$$p = -\rho\frac{D\phi}{Dt} \tag{2}$$

where $\frac{D\phi}{Dt}$ is the substantive derivative. Dropping out the second order terms and integrating with respect to observer time results in

$$\phi(t) = \int_{-\infty}^{t} \Psi(t')\, dt' \tag{3}$$

$$\Delta w_n = \frac{\partial\phi}{\partial n} = \frac{\partial}{\partial n}\int_{-\infty}^{t} \Psi\, dt'\, dA' \tag{4}$$

The right hand side of Eq. (4) represents an induced velocity in the direction $\vec{n}$ due to a moving source (or doublet) of strength q where q is contained in the expression for Ψ. By summing the contribution of all doublets distributed over the rotor, the induced velocity along $\vec{n}$ at the downwash point can be represented as

$$w_n = \int \Delta w_n\, dA' = \int \frac{\partial}{\partial n} \int_{-\infty}^{t} \Psi\, dt'\, dA' \tag{5}$$

The left hand side, w_η, represents the known boundary condition and is the velocity normal to the velocity vector at the downwash point. Thus the problem resolves itself into setting up a method of solution of equation (5) from which the values of q, the unknown, can be determined which satisfy the known velocity boundary conditions w_η. The next section contains the development of the expression for an acceleration doublet potential.

Acceleration Potential of a Doublet in Compressible Flow

The acceleration potential Ψ_S must satisfy the wave equation

$$\nabla^2\Psi_S - \frac{1}{c^2}\frac{\partial^2\Psi_S}{\partial t^2} = f(\vec{X},t)$$

where $f(\vec{X},t)$ is a source distribution. Furthermore, if the path of an isolated source is a function of time $\vec{X}_O(t)$, then $f(\vec{X},t) = q\delta(\vec{X} - \vec{X}o(t))$ where δ is the Dirac delta function.

Using the Green's function formulation the acceleration potential expression for a moving source, Ψ_S can be written as (Morse and Feshbach, 1978, page 841)

$$\Psi_S(\vec{X},t) = \frac{q(\vec{X}_0,\tau)}{4\pi\left|\vec{X} - \vec{X}_0(\tau)\right|\left|1 - \dfrac{\vec{V}_0(\tau)\cdot[\vec{X} - \vec{X}_0(\tau)]}{c\left|\vec{X} - \vec{X}_0(\tau)\right|}\right|} \tag{6}$$

where $\vec{X}_0(\tau)$ designates the position of the source at time τ, $\vec{X}$ is the position of the field point at the time t, $V_0(\tau)$ is the velocity of the source point at time τ, c is the speed of sound and q is the strength of the source. An auxiliary equation which relates the time interval $(t - \tau)$ to the distance

$$t - \tau = \frac{\left|\vec{X} - \vec{X}_0(\tau)\right|}{c} \tag{7}$$

which is usually referred to as the causality condition. Eq. (6) expresses the potential as function of τ, and only though Eq. (7) as an implicit function of t and $\vec{X}$.

From Eqs. (3) and (6), the velocity potential due to a moving source is

$$\begin{aligned}\phi_S(t) &= \int_{-\infty}^{t} \Psi_S(t')\,dt' = \int_{-\infty}^{t} \frac{q(\tau')}{4\pi\left|D - \vec{D}\cdot\vec{\beta}\right|_{t'}}\,dt' \\ &= \frac{1}{4\pi}\int_{-\infty}^{\tau} \frac{q(\tau')}{D(\tau')}\,d\tau',\end{aligned} \tag{8}$$

where $\vec{D} = \vec{X} - \vec{X}$, $D = \left|\vec{D}\right|$ and $dt' = \left[1 - \dfrac{\vec{D}\cdot\vec{\beta}}{D}\right] d\tau'$. The quantities τ', t' and t, τ satisfy eq. (7).

A source potential cannot be used to produce a pressure difference across a lifting surface. However, a doublet does contain the proper form of the singularity on the surface to provide a jump in pressure over such a lifting surface. The expression for a doublet potential can be obtained by taking the derivative of a source potential in a direction normal to the airfoil surface. If $\vec{n}_0$ designates the normal to the airfoil surface, then

$$\begin{aligned}\phi_D(t) &= \frac{\partial}{\partial n_0}\phi_S(t) = \vec{n}_0 \cdot \nabla_{\vec{X}_0}\phi_S = -\,\vec{n}_0 \cdot \nabla_{\vec{X}}\phi_S \\ &= \frac{\vec{n}_0 \cdot \vec{D}}{4\pi c(D - \vec{\beta}\cdot\vec{D})}\frac{q}{D}\Big|_{\tau} + \int_{-\infty}^{\tau} q\,\frac{\vec{n}_0 \cdot \vec{D}}{4\pi D^3}\,d\tau'\end{aligned} \tag{9}$$

Eq. (9) was also derived by Dat (1973) in a different fashion. Note that for incompressible flow, $c \to \infty$, the first term $\to 0$ and

The integral remains unchanged except for the upper limit where $\tau = t$.

To obtain the final equation for downwash Δw_n, a second directional derivative is required. This derivative is taken normal to the flight path at the location of the downwash point,

$$\Delta w_n = \frac{\partial \phi_D}{\partial n} = \vec{n} \cdot \nabla_{\vec{x}} \phi_D$$

This leads to

$$\Delta w_n = \frac{q}{4\pi c D^2 [1-\hat{D} \cdot \vec{\beta}]} \left[[\vec{n} \cdot \vec{n}_o - \vec{n}_o \cdot \hat{D}\, \vec{n} \cdot \hat{D}] \right.$$

$$+ \frac{\vec{n}_o \cdot \vec{\beta}\, \vec{n} \cdot \hat{D} - \frac{\vec{D}}{c} \cdot \dot{\vec{n}}_o\, \vec{n} \cdot \hat{D} - \vec{n}_o \cdot \hat{D}\, \vec{n} \cdot \hat{D} + \vec{n}_o \cdot \hat{D}\, \vec{n} \cdot \vec{\beta}}{(1 - \hat{D} \cdot \vec{\beta})} \quad - (10)$$

$$\left. \frac{\vec{n}_o \cdot \hat{D}\, \vec{n} \cdot \hat{D}[1-\beta^2 + \frac{\vec{D}}{c} \cdot \dot{\vec{\beta}}]}{(1 - \hat{D} \cdot \vec{\beta})^2} \right] \Bigg|_{\tau_o} - \frac{\vec{n}_o \cdot \hat{D}\vec{n} \cdot \hat{D}\, \dot{q}}{4\pi c^2 D\, [1 - \hat{D} \cdot \vec{\beta}]^2} \Bigg|_{\tau_o}$$

$$+ \frac{1}{4\pi} \int_{-\infty}^{\tau_o(r_o)} q \left[\frac{\vec{n} \cdot \vec{n}_o - 3\vec{n}_o \cdot \hat{D}\vec{n} \cdot \hat{D}}{D^3} \right] d\tau$$

This concludes the derviation of the basic equation for the downwash Δw_n at a field point created by an arbitrarily moving doublet. In the present application, the term containing $\dot{q}$ was not used in the subsequent calculations. It can be argued that the ratio of the $\dot{q}$ term to the fifth term in the first bracket is $\Omega D/C$ which is small unless the frequency, Ω, is very large which might be true in other applications such as acoustics. The remaining portion of the paper is directed towards specializing this equation for a helicopter blade, moving with a forward velocity U, a vertical velocity W, and rotating with angular velocity Ω.

Equation (10) gives the downwash at a field point (x, y, z, t) due a doublet placed at a point (x_o, y_o, z_o, τ) having a strength q. In order to form a lifting surface such as a rotor, it is necessary to distribute the doublets over the lifting surface and integrate over the surface to obtain the downwash at a field point. If the downwash is known, the quantity "q" then can be determined. Letting K be the expression on the right hand side of equation (10), the final equation is

$$w_n = \iint_{A'} K \, dA' \qquad (11)$$

where A' is the area of the rotor surface. This represents a rather formidable computing task and the history of lifting surface theory even for non-rotating wings has centered on

devising approximate methods to accomplish the integration in an economical manner. One method, termed the doublet lattice method, has been very successfully applied to aircraft wings, and is probably the more economical procedure of the many variants. This method was first demonstrated for the unsteady case by Runyan and Woolston (1957) and was later expanded by Albano and Rodden (1969). This is the method adopted in this paper and the application will be discussed later. In the next section the coordinate system is specified and the doublets and downwash points are appropriately located for a helicopter rotor in forward flight.

Specification of Coordinate System

The blade has the cord C and length $R_t - R_s$, R_s being the radial distance to the the root of the blade, R_t is the distance to the tip of the blade. The blade executes a counterclockwise rotation with angular velocity Ω while moving with velocity U along the negative x direction and W along the positive z direction. Since the doublet lattice method has been adopted, for one chordwise panel, the doublet point lies 1/4 C ahead and the downwash point lies 1/4 C aft of the midchord. The position of the doublet point as well as the downwash point can be established as follows. The Cartesian components of the doublet position are

$$\begin{aligned} x_0 &= -U\tau + r_0 \cos(\Omega\tau) - (C/4)\sin(\Omega\tau)\cos\alpha_0 \\ y_0 &= r_0 \sin(\Omega\tau) + (C/4)\cos(\Omega\tau)\cos\alpha_0 \\ z_0 &= W\tau + (C/4)\sin\alpha_0 \end{aligned} \tag{12a}$$

where r_0 is the radial distance of the doublet along the span. With the substitution of $C \to -C$, $r_0 \to r$, $\tau \to t$ the position of the downwash point is given by

$$\begin{aligned} x &= -Ut + r\cos(\Omega t) + (C/4)\sin(\Omega t)\cos\alpha \\ y &= r\sin(\Omega t) - (C/4)\cos(\Omega t)\cos\alpha \\ z &= Wt - (C/4)\sin\alpha \end{aligned} \tag{12b}$$

In eqs. (12), the angles α, α_0 are the twist angles of the velocity vectors $\vec{V}$ and $\vec{V}_0$, respectively, defined by

$$\begin{aligned} \tan\alpha &= \frac{W}{U\sin(\Omega t) + r\Omega} \\ \tan\alpha_0 &= \frac{W}{U\sin(\Omega\tau) + r_0\Omega} \end{aligned} \tag{13}$$

The vector $\vec{D} = \vec{X} - \vec{X}_0$ defined in Eq. (8) can be expressed as

$$\begin{aligned} D = \{&[U(t-\tau) + r\cos(\Omega t) - r_0\cos(\Omega\tau) + (C/4)(\sin(\Omega t)\cos\alpha + \sin(\Omega\tau)\cos\alpha_0)]^2 \\ &+ [r\sin(\Omega t) - r_0\sin(\Omega\tau) - (C/4)(\cos(\Omega t)\cos\alpha + \cos(\Omega\tau)\cos\alpha_0)]^2 \\ &+ [W(t-\tau) - (C/4)(\sin\alpha_0 + \sin\alpha)]^2\}^{1/2} \end{aligned}$$

The integral equation was solved for the unknown $q(r_o,\tau)$ by using a collocation process based on the doublet lattice assumption. The kernel is singular when D = 0, and this was handled by use of the finite part technique.

SOLUTION OF INTEGRAL EQUATION

Equation (11) states that doublets of strength "q" are distributed over the area of the rotor surface A' and the induced velocity normal to the blade surface is equated to the normal velocity of the blade, w_n, where w_n is the boundary condition on the blade surface and is a known quantity. Thus, the only unknown in the integral equation is the strength of the doublet, q. As mentioned previously, one method for obtaining a solution to this equation is termed the doublet lattice method, and is the method used in this report. It has been used successfully for the wing in pure translational motion. One of the advantages of the doublet lattice method is that it eliminates the chordwise integration, thus reducing computing costs. The reduction is the result of a judicious choice of the location of the doublet and the downwash points.

Doublet Lattice Technique

In following the doublet lattice technique the rotor is divided into a number of panels, both spanwise and chordwise. In each panel, a line of doublets of unknown strength q_j is located at the 25% chordwise location of the particular panel, and the downwash is evaluated at the point located at 75% chordwise location and midspan of the panel. The problem then resolves itself into performing an integration from r_ℓ to r_u for the vortex located at C/8 for the downwash point located in the middle of the spanwise panel at (3/8)C (w_n=w_1) and the effect of the same vortex must be determined for the downwash located at (7/8)C ($w_n = w_2$). A similar calculation is made for all the remaining vortices including lateral distances. Therefore, a collocation procedure is used to obtain a set of equations in terms of the unknown loadings q_j.

The term $q(r_o,\tau)$ represents the strength of the doublet located at r_o and at time τ, and is proportional to the unknown loading. Within a particular panel, q is assumed to be constant in the spanwise direction. In order to account for unsteadiness, a solution was formulated to take into account the time variation of the strength of the doublet. The time variation of q is represented by assuming a Fourier series of the form

$$q(r_o,\tau) = A_o(r_o) + \sum_{1}^{m} (A_n(r_o)\cos(n\Omega\tau) + B_n(r_o)\sin(n\Omega\tau)) \quad (14)$$

If $q(r_o,\tau)$ is assumed to be a function of r_o alone, which means that the doublet strength does not vary with time, the Fourier series reduces to $q(r_o) = A_o$. A solution obtained with this approximation is termed the quasi-steady solution.

This series was inserted in the basic equation (Eq. (11)) and integrated with respect to τ. However, there were more unknowns than simultaneous equations to solve for the unknowns.

The additional required equations were obtained by evaluating Eq. (11) at a number of azimuth locations. For instance if m = 1, then

$$q(r_o,\tau) = A_o + A_1 \cos(\Omega\tau) +_1 B \sin(\Omega\tau) \qquad (15)$$

The azimuth was divided into equal segments of 120° and the proper boundary conditions applied at ψ = 0°, 120°, and 240° thus providing the necessary additional equations.

A set of equations is thus obtained as shown below

$$\begin{aligned} w_1 &= A_{11}q_1 + A_{12}q_2 + \cdots \quad A_{1m}q_m \\ w_2 &= A_{21}q_1 + A_{22}q_2 + \cdots \quad A_{2m}q_m \\ w_n &= A_{n1}q_1 + A_{n2}q_2 + \cdots \quad A_{nm}q_m \end{aligned} \qquad (16)$$

where $A_{nm} = \int_{r_\ell}^{r_u} K_{nm}\, dr_o$ and where n refers to the downwash point and m refers to the panel number. The rotor can be divided into any number of segments both chordwise and spanwise, with more segments resulting in more accurate results. However, the computing time and costs increases rapidly (roughly proportional to the square of the numbers of segments) as the number of segments is increased, thus a balance must be considered in any given situation, trading computing costs with desired accuracy.

Numerical Integration of Kernel

A closed form integration of the kernel has not been found, therefore the integration was performed by numerical integration, except for the area surrounding the singularity. The integral over areas not containing the singularity were computed numerically using two-dimensional Romberg quadrature (Davis and Rabinowitz, 1984) and the contribution of the singular region was obtained in closed form by consideration of the finite part as shown in the next section.

Treatment of Singular Term in Integral - The integral in the downwash equation, Eq. (10), is singular when D→0 and produces a complication which must be properly treated. It should be remembered that the integration path along "τ" is the path the doublet has taken in arriving at the final doublet point at (c/4, r_o) measured in the local blade coordinates. The integration takes place along the path from τ=-∞ to the final doublet position at τ_o. The distance D is the distance from the integration point at time τ to the downwash point at $\vec{X}$.

There is a particular set of values of r_o and τ for which the denominator D approaches zero, thus resulting in an infinite integrand. The singular part of the kernel is

$$I = \int_{r_\ell}^{r_u} \int_{\tau_1}^{\tau_2} \frac{\vec{n}\cdot\vec{n}_o - 3(\hat{D}\cdot\vec{n})(\hat{D}\cdot\vec{n}_o)}{D^3} \, d\tau_o \, dr_o \qquad (17)$$

As $D \to 0$ at the downwash point, $\hat{D}$ becomes perpendicular to $\vec{n}$, therefore, at the singular point, the second term is zero and will be neglected in the treatment of the singularity. However, this second term is retained in all of the numerical integrations since it represents an important interference term, particularly when the blade is passing over a trailing wake.

APPLICATION TO SPECIFIC EXAMPLES

The foregoing analysis has been applied to several specific examples which are given in Fig. 2. The following section presents results for several paneling configurations; e.g. 5 spanwise and 1 chordwise panels (designated (5-1)) and 7 spanwise and 3 chordwise (designated (7-3)). The untwisted rotor blade was maintained at a constant pitch setting of $\theta_B = 0.1$ radians for all the calculations. Although the spacing of the paneling can be arbitrary, the paneling arrangements used in all following examples are uniform except for the swept tip cases where the arrangement is described.

Incompressible Flow

Single Blade

In order to investigate the convergence of the method when using the doublet lattice procedure, the program was run for several chordwise and panwise elements for the incompressible case. The thrust coefficients C_T vs. the azimuth angle is shown in fig. (3). (In all of the follow plots for thrust coefficient vs. azimuth angle, the thrust was calculate for 16 uniformly spaced azimuth angles and each curve was faired using a cubic spline). The rotor was first divided into 5 spanwise and one chordwise panel (5-1) and the results are shown by the solid line. The chordwise divisions were increased to (5-2) and the results are shown by the long dashed line. It can be seen that very little change has taken place. The spanwise divisions were increased to (7-1) and the largest change between various paneling schemes occurred at $\psi = 0^o$ where the difference in C_T is about 11%. Increasing the chordwise divisions to 3 (7-3) produced a little change from the (7-1) case.

An interesting phenomena occurs in the rotor first quadrant. For ψ=0 to 37^o, the lift increases to a local maximum at ψ=37^o then the lift abruptly falls to a local minimum for ψ=60^o and then rapidly increased to a maximum at ψ=100^o. A similar phenomenon is shown analytically by Egolf and Landgrebe (1983) in Fig. 60 of that report where a local minimum and a local maximum occur in the same range of azimuth angles, even though the geometry of the two blades and the flight conditions are different. Also, in Fig. 93 of the same report some test data shows a similar variation of loading in the same azimuth range.

The chordwise pressure distributions for the (7-3) case are presented in figure 4. It should be remembered that in using the doublet lattice method, the loading is concentrated at the

location of the doublet which for the (7-3) case is located at 0.0833C, 0.416C, and 0.75C. The pressure was faired using a cubic spline through the three vortex locations and the known value of zero at the trailing edge. The distributions are given for 7 spanwise positions. In general, the curves exhibit the expected shape, having the largest values as the leading edge is approached. For the span distribution the values at r/R_T = .85 are slightly larger than the values at r/R_T = 0.95, indicating a falling off in the tip region.

Swept Tip

The segments used for the doublet lattice for the swept tip studies were(5-1), where two equal segments were used in the tip region and three equal segments were used in the unswept inboard section. In Fig. 5 the lift is shown plotted against azimuth for the two sweep conditions and for zero sweep. In general, the three results show little difference. The sweptback configuration has the largest lift from $\psi \approx 300^o$ to 40^o. For $\psi \approx 100^o$ to 240^o, the swept forward configuration has a slightly larger lift than the other configurations. It appears that the total lift for one rotation for the swept-back case and the sweptforward case would give about the same lift as produced by the unswept rotor. In Fig. 6 the lift distribution along the rotor span is given for $\psi = 0^o$. The major effect of sweep is concentrated at the tip, where the swept-back tip load is greater than either the unswept or sweptforward cases. In contrast, for $\psi = 180°$, Fig. (7) shows the swept forward tip load to be larger than for the unswept or sweptback tip.

Blade Oscillating in Pitch

An example of unsteady loads on a rotor blade with (5-1) paneling which is oscillating in a pitching mode about the mid-chord at a frequency of 4 per revolution (120 cycles/sec) is given on fig. 8. For this case a 17 term Fourier series (m=8) was used to simulate the oscillating load, which was comprised of one constant term, 8 cosine terms, and 8 sine terms. The non-oscillatory and oscillating rotor blade loading is given for one revolution. The blade was oscillated through an angle of ±0.1 rad. about a mean angle of 0.1 rad. The effect of the oscillation is readily apparent as compared to the non-oscillatory case. With the harmonic representation of the loading, the magnitude and phase of the several harmonic loads are easily determined. The magnitudes are plotted in Fig. 9. The only harmonic loads that were significantly changed from the steady case were the 3rd, 4th and 5th. Both the 3rd and 5th harmonics were increased and the 4th harmonic was dramatically increased. Another calculation was made for the non-oscillatory case and compared to the quasi-steady case. Virtually no difference was observed, indicating that, at least for this case, the rate of change of loading in a revolution of the blade is small enough so that the effect of a variable wake is negligible.

Parametric Study Involving Horizontal Velocity U and Vertical Velocity W

In the next two figures, results of a parametric study involving variations of the horizontal velocity U and the velocity W are given. In figure 10, the thrust coefficient C_T

is plotted against azimuth angle for a constant horizontal velocity U = 100 ft/sec. and for several values of the vertical velocity W. (It should be recalled that in the coordinate system used in this paper, the rotor blades rotate in a plane parallel to the horizontal plane and move in the negative X-direction with velocity U and moves vertically with velocity W. Therefore, the total forward velocity is $\sqrt{U^2 + W^2}$ and if this total velocity is taken as horizontal, the tip path plane is tilted by $\alpha_r = \tan\left(\frac{W}{U}\right)$.) For positive values of W, the tip path plane is such that a propelling thrust is created, whereas a negative W would represent a stopping or retarding thrust. The largest values of C_T are found for the negative W which is to be expected since negative values of W represents an increase in blade angle of attack. Note that the notch in C_T that occurs in the range of ψ = 45° to 60° for W = -5 ft/sec. to +10 but does not appear for W = 20 ft/sec. In general, there is an orderly progression in C_T as the values of W are changed.

In figure 11, where C_T is plotted against azimuth angle, the forward velocity was varied from U = 100 ft/sec. to U = 10 ft/sec. Contrary to the previous figure, the results for the three horizontal velocities show significant differences. For instance, for U = 100 ft/sec., C_T is substantially greater than for U = 50 or 10 ft/sec. in the range of ψ = 90 to 120°, whereas in the range of ψ = 200° to 300°, the thrust coefficient is the lowest for U = 100 ft/sec.

Compressible Flow

One-Blade Rotor (5-1)

For a one-bladed rotor, the effect of compressibility is illustrated in Fig. 12, in which the C_T is plotted against azimuth angle. The incompressible result is included for comparison. As expected, the compressible load is larger than the incompressible throughout one revolution. The effect is greatest in the region of the advancing blade and smallest in the retreating region as would be expected.

Two-Bladed Rotor (5-1 per blade)

The method has been extended to the two-bladed rotor for the compressible case and the results are shown in Fig. 13. The thrust coefficient C_T, per blade is given vs. azimuth angle for a single bladed rotor and for a two-bladed rotor. For azimuth angles from $\psi = 20^0$ to 120^0 the single-blade rotor has a larger C_T. For $\psi = 120^0$ to 260^0, the C_T on the one-and two-bladed rotors are approximately the same. However, for $\psi = 260^0$ to 340^0 a dramatic reduction in lift per blade occurs for the two-bladed rotor as compared to the one bladed results. The lowest lift occurs at $\psi = 292^0$ which places the other blade of the two-bladed rotor at $\psi = 112^0$, the point of maximum lift on the other blade. Apparently the high lift on the blade at $\psi = 112^0$ creates a very unfavorable induced velocity on the second blade at $\psi = 292^0$ which requires the loading to go to zero in order to satisfy the boundary conditions at $\psi = 292^0$.

Comparison of Theory with Experiment

In figure 14, a comparison between the present theory and a model experiment, reference Meyer et al, 1953, is given. The experiment employed a two-bladed rotor. The rotor radius was 2.5 ft., the chord was 1/4 ft. and the rotation rate was 83.8 radius/sec. The forward velocity was 45.8 ft/sec. No cyclic pitch was induced. The lift force on each blade in pounds/in. is plotted against span position. For the blade located at Ψ = 150°, the theory is about 9% lower than the experiment in the neighborhood of the peak load. For Ψ = 330°, the agreement is excellent. Thus it appears that the theory appears to be adequate for predicting airloads.

CONCLUDING REMARKS

A linearized lifting surface theory including the effects of compressibility has been developed for a helicopter rotor in forward flight. The method utilizes the concept of the acceleration potential, and makes use of the vortex-lattice procedure for performing the required integrations. In addition, the method has been extended to include the effects of unsteady flow, and blade deformation.

Sample calculations have been done for several cases. These include the effect of a swept-back and a swept-forward tip. The effect of these two tip configurations was minimal on the total loading for one revolution. However, the loading distribution changed considerably for several azimuth positions. Compressibility was investigated for one configuration. As expected, the effect was greatest in the advancing blade region ($\psi = 90^0$) and was minimal in the retreating blade region. A comparison of the thrust coefficient, C_T, of a one bladed rotor and a two bladed rotor was made. In the azimuthal range between 20^0 and 120^0, the one bladed rotor showed higher lift. However between $\psi = 260^0$ to 340^0 the two bladed rotor indicated a lower C_T. The effect on C_T of a blade oscillating in pitch at 4/rev is given. The effect on the total blade lift is shown and the effect of the oscillation is readily apparent. The harmonic content was calculated and the greatest difference between the oscillatory and non-oscillatory cases was found in the 4th harmonic.

Finally, a comparison between the present theory and an experiment for a two bladed rotor is given and the agreement was found to be excellent.

REFERENCES

Albano, E.; Rodden, W. P. 1969: A Doublet Lattice Method for Calculating Lift Distribution on Oscillating Surfaces in Subsonic Flows. AIAA Journal, Vol. 7, No. 2, pp. 279-285.

Costes, J. J., 1972: "Calcul des forces aerodynamiques instationnaires sur les pales d'un rotor d'helicoptere". La Recherche Aerospatiale, No. 1972-2. English translation NASA TT.F15039 (1973). See also AGARD Report No. 595.

Davis, P. J. and Rabinowitiz, P., 1984: Methods of Numerical Integration, Academic Press

Dat, Roland 1973: The Lifting Surface Theory Applied to Fixed Wings and Propellers. ONERA TP No. 1298.

Egolf, T. A., and A. J. Landgrebe, 1983: Helicopter Rotor Wake Geometry and Its Influence in Forward Flight, Volume I - Generalized Wake Geometry and Wake Effect on Rotor Airloads and Performance, NASA CR-3726, Volume II - Wake Geometry Charts, NASA CR 3727.

Meyer, John, Jr., and Falabella, Gaetano, Jr., 1953: NACA TN-2953, Fig. 23.

Pierce, G. A.; and Vaidyanathan, A. R. 1983: Helicopter Rotor Loads Using Discretized Matched Asymptotic Expansions, NASA CR 166092.

Runyan, H. L., and Woolston, D. S. 1957: Method for Calculating the Aerodynamic Loading on an Oscillating Finite Wing in Subsonic and Sonic Flow. NACA TR 1322.

Runyan, H. L. 1973: Unsteady Lifting Surface Theory Applied to a Propeller and Helicopter Rotor, Ph.D. Thesis, Loughborough, University of Technology.

Suciu, E. O., Preuss, R. D. and Morino, L., 1976: Computational Aerodynamic Analysis of Horizontal-Axis Windmills, Boston University, Engr-CCMP-Tr-76-01.

Van Holten, T. H., 1975: The Computation of Aerodynamic Loads on Helicopter Blades in Forward Flight, Using the Method of the Acceleration Potential. Rep. VTH-189, Technische Hogeschool Delft, Netherlands.

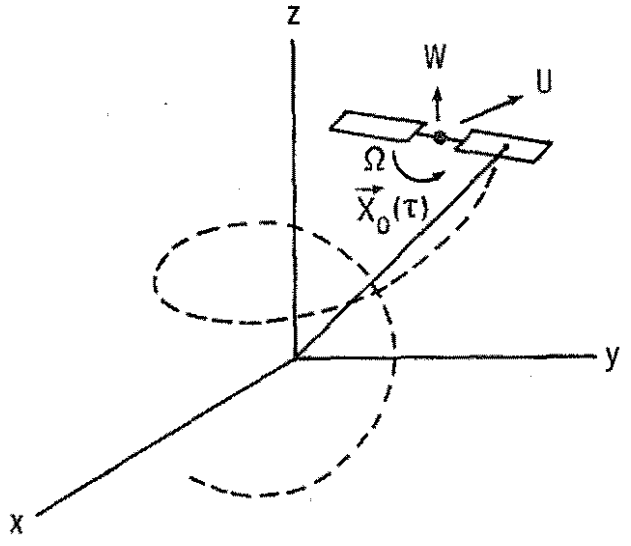

Fig. 1 Inertial Coordinate System

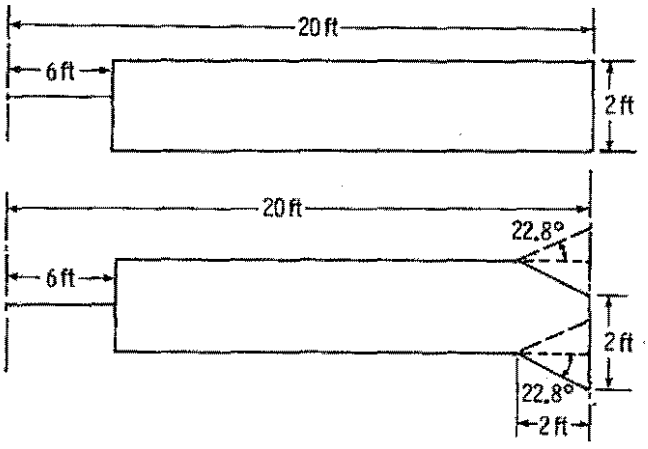

U = 100 ft/sec $\quad \alpha_r = 0.05$ rad
W = 5 ft/sec
Ω = 30 rad/sec $\quad \mu = 0.17$

Fig. 2 Configurations and Input Parameters used in examples

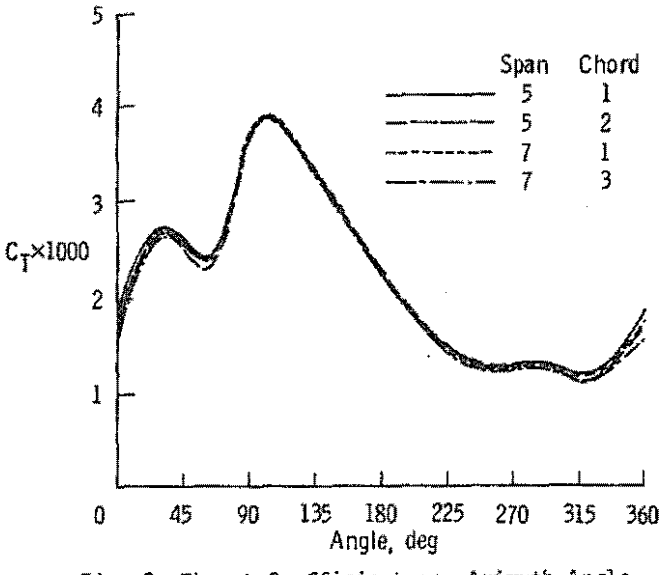

Fig. 3 Thrust Coefficient vs. Aximuth Angle for Four Panel Configurations for a Single Rotor Blade, incompressible, (μ = 0.17, θ_β = 0.1 rad, α_r = .05 rad, Ω = 30 rad/sec)

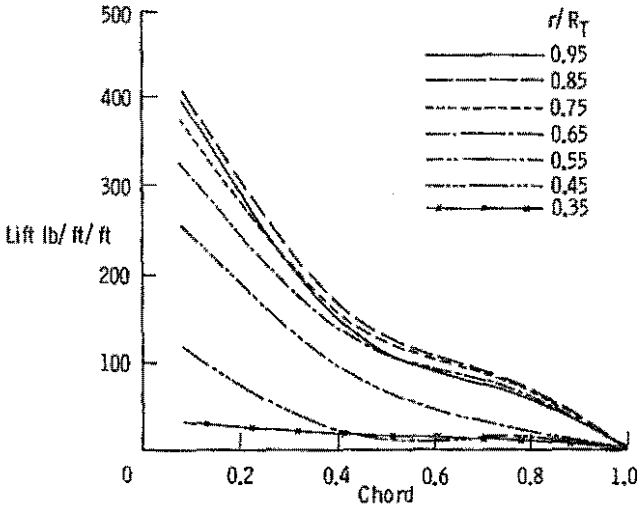

Fig. 4 Chordwise Pressure Distribution for Several Spanwise Locations, Ψ = 90°, incompressible, (μ = .17, θ_β = 0.1 rad, α_r = .05 rad, Ω = 30 rad/sec)

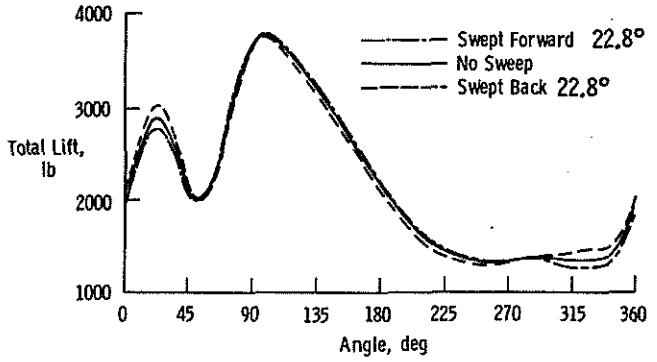

Fig. 5 Comparison of Lift on a Swept-Back Zero Sweep and Swept-Forward Blade, incompressible, (μ = 0.17, θ_β = 0.1 rad, α_r = .05 rad, Ω = 30 rad/sec)

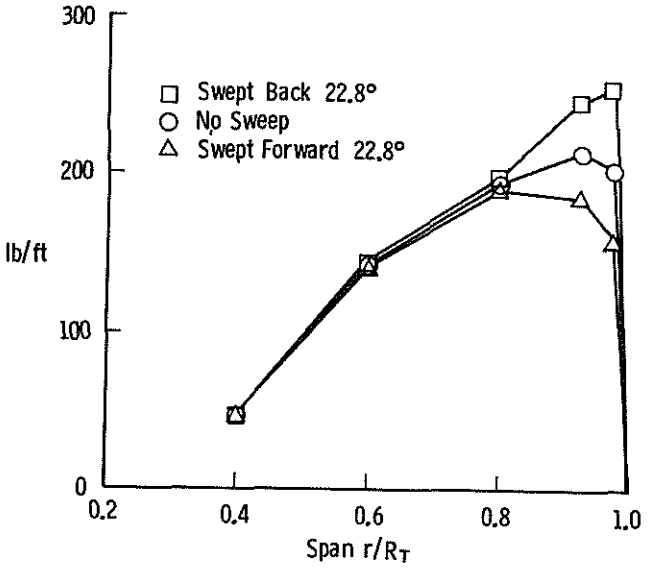

Fig. 6 Spanwise Section Lift Distribution for Swept-Tip Configurations, Ψ = 0°, incompressible, (μ = 0.17, θ_β = 0.1 rad, α_r = .05 rad, Ω = 30 rad/sec)

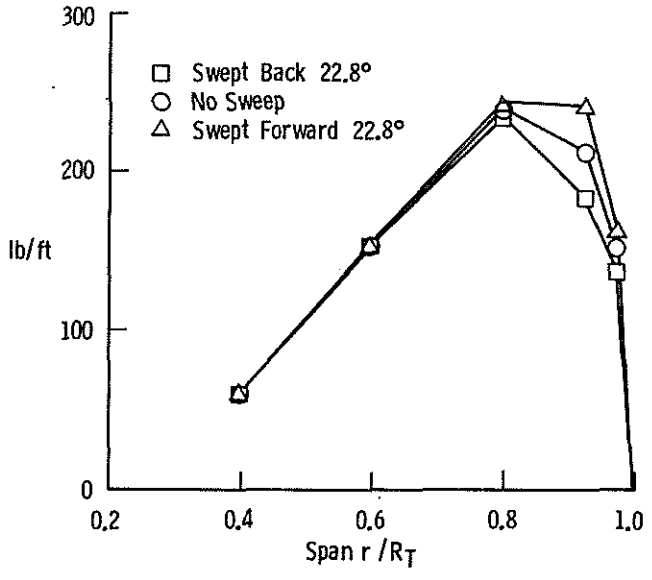

Fig. 7 Spanwise Section Lift Distribution for Swept-Tip Configurations, Ψ = 180°, incompressible, (μ = 0.17, θ_β = 0.1 rad, α_r rad, Ω = 30 rad/sec)

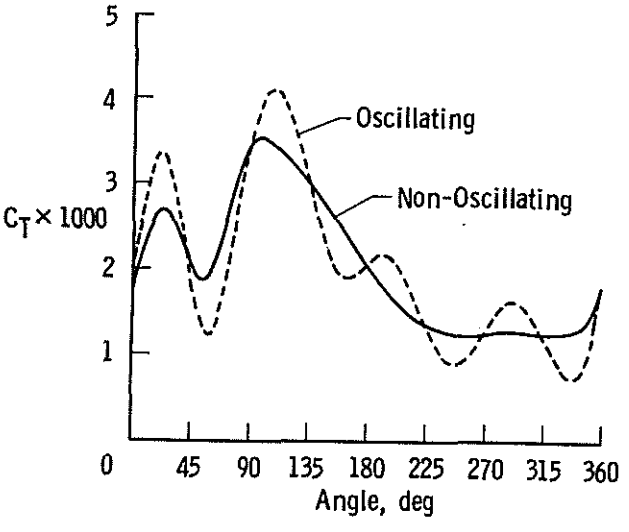

Fig. 8 Comparison of Lift on a Rotor Blade Oscillating in Pitch at 4/Rev. to the Lift on a Non-Oscillatory Blade, incompressible (μ = 0.17, θ_β = 0.1 rad, α_r = .05 rad, Ω = 30 rad/sec)

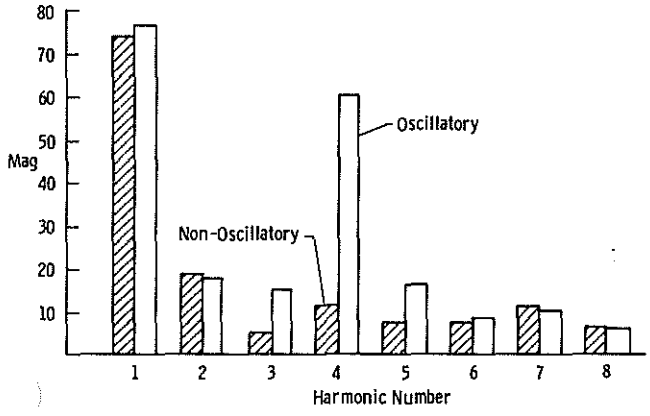

Fig. 9 Harmonic Content for Non-Oscillatory and Oscillatory Cases - r/R_T = .95, incompressible, (μ = 0.17, θ_β = 0.1 rad, α_r = .05 rad, Ω = 30 rad/sec)

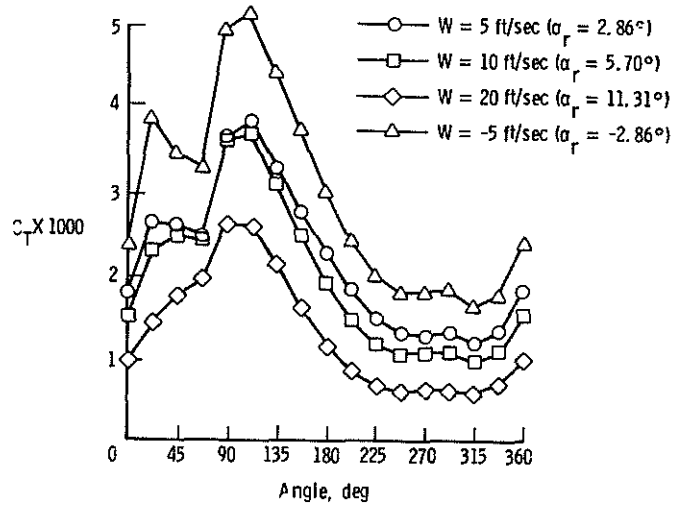

Fig. 10 Thrust coefficient of a single blade rotor for several vertical velocities (W) with horizontal velocity held constant, Ω = 30 rad/sec, U = 100 ft/sec

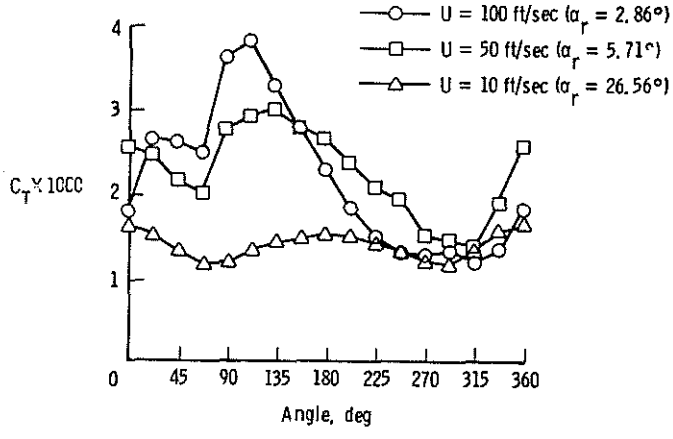

Fig. 11 Thrust coefficient of a single blade rotor for a constant vertical velocity (W = 5 ft/sec) with varying forward speed, Ω = 30 rad/sec

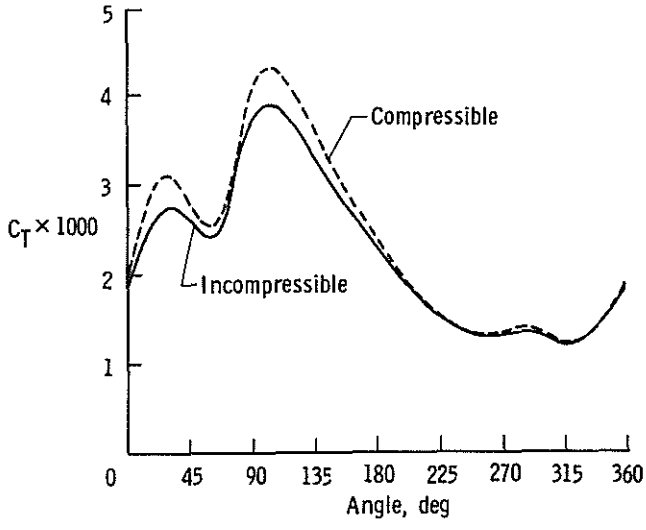

Fig. 12 Incompressible and Compressible Lift for One-Bladed Rotor, (μ = 0.17, θ_β = 0.1 rad, α_r = .05 rad, M_{TIP} = 0.54

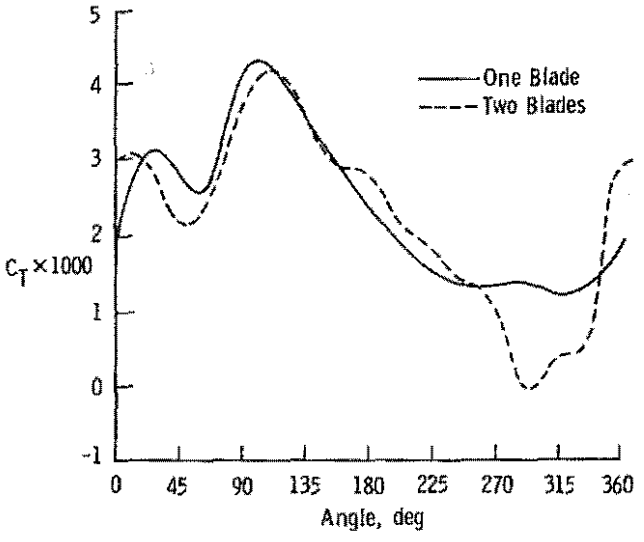

Fig. 13 Lift on Two-Bladed and One-Bladed Rotor vs. Azimuth Angle, compressible, $\mu = 0.17$, $\theta_\beta = 0.1$ rad, $\alpha_r = .05$ rad, $M_{TIP} = 0.54$

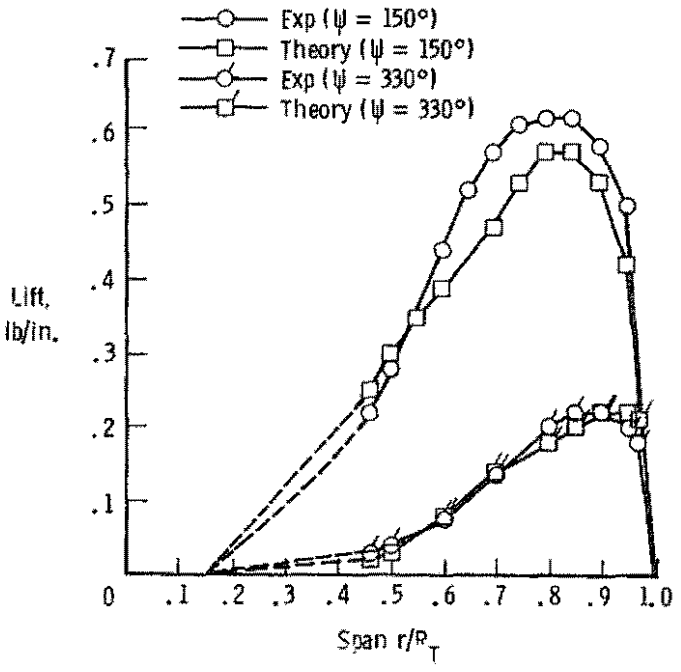

Fig. 14 Comparison of experimental and theoretical spanwise lift distribution